14th International Conference on Structural Safety and Reliability - ICOSSAR'25
1-6 June, 2025 - Los Angeles California, USA
R. Ghanem, E. Johnson, S. Masri and A. Olivier (Eds)

INFLUENCE OF PRIOR ON ESTIMATION RESULTS IN SIMULTANEOUS GEOMETRY AND SPATIAL FIELD ESTIMATION

TATSUYA SHIBATA[1,*], MICHAEL C. KOCH[1], IASON PAPAIOANNOU[2] and KAZUNORI FUJISAWA[1]

[1] Graduate School of Agriculture, Kyoto University
Kitashirakawa-oiwakecho, Sakyo-ku, 606-8502 Kyoto, Japan
[*] shibata.tatsuya.84z@st.kyoto-u.ac.jp

[2] Engineering Risk Analysis Group, Technische Universität München
Arcisstr. 21, 80290 München, Germany

Key words: Inverse problems, Interface detection, Karhunen–Loève expansion, Hyperparameter

1 INTRODUCTION

The visualization of subsurface structures is typically achieved by estimating the spatial field of physical properties from the related measurement data. In most cases, observations used for estimation are noisy and limited, resulting in uncertain estimation results. The Bayesian approach is an effective method for addressing this uncertainty. In the Bayesian framework, the spatial field of physical properties is called a random field and is efficiently parameterized using the Karhunen–Loève (K-L) expansion [1], which reduces the dimensionality of the random field. For tractability, a Gaussian random field is chosen as the prior of the random field, resulting in normally distributed coefficients in the Karhunen–Loève expansion. However, while this approach works well for smoothly varying fields, it has limitations in sharply detecting interfaces where physical properties change abruptly, such as buried objects, cavities, or cracks. This limitation arises from the spatial correlation assumption in Gaussian processes. Specifically, a large correlation length leads to overly smooth estimates that fail to capture sharp changes, while a small correlation length increases variance, resulting in unstable estimates. These issues make it difficult to achieve both dimensionality reduction and accuracy in interface detection.

To overcome this difficulty, we previously proposed a method that explicitly introduces geometry parameters related to buried anomalies and estimates them simultaneously with the background spatial field [2, 3]. This simultaneous estimation allows for sharp interface detection while preserving the dimensionality reduction advantages of the K–L expansion. At first consideration, this approach seems to be computationally expensive because the domain changes with each update of the geometry parameters, and the eigenvalue problem must be solved each time for constructing the K-L expansion [2]. However, by taking advantage of the domain-independent property [4] of the K-L expansion, the eigenvalue problem only needs to be solved once for a fixed bounding domain, and the introduction of geometry parameters is not a computational bottleneck. Furthermore, since the eigenpairs remain fixed, gradient computation becomes straightforward, allowing for the easy implementation of Hamiltonian Monte Carlo (HMC) [5], which enables efficient sampling.

The main contribution of this study lies in clarifying the influence of prior selection on the accuracy of simultaneous geometry and spatial field estimation within a Bayesian framework. By systematically analyzing hyperparameter settings, this work provides practical guidelines for enhancing interface detection in inverse problems. Particular attention is given to the correlation length of the prior Gaussian random field and the variance of the geometry parameters. An inverse problem for one-dimensional seepage flow is solved using several sets of hyperparameters, and the results are compared.

The remainder of this paper is organized as follows. In Section 2, the parameterization of the simultaneous estimation is explained. Section 3 describes the framework of Bayesian inference briefly. In Section 4, the numerical study of inverse analysis for 1D seepage flow is presented.

2 MODELING OF INVERSE PROBLEM

2.1 Karhunen–Loève expansion

Let us consider a Gaussian random field $X(\mathbf{z})$ with mean $\overline{X}(\mathbf{z})$ and covariance kernel $C(\mathbf{z}, \mathbf{z}^*)$. Let $\{\lambda_i, \phi_i\}_{i=1}^{\infty}$ be the eigenpairs of the integral eigenvalue problem (IEVP) defined over $\mathcal{D}'$ as follows:

$$\int_{\mathcal{D}'} C\left(\mathbf{z}, \mathbf{z}^*\right) \phi_i(\mathbf{z}^*) \mathrm{d}\mathbf{z}^* = \lambda_i \phi_i(\mathbf{z}). \tag{1}$$

Then, according to Mercer's theorem, $C\left(\mathbf{z}, \mathbf{z}^*\right) : \mathcal{D}' \times \mathcal{D}' \to \mathbb{R}$ can be represented as

$$C\left(\mathbf{z}, \mathbf{z}^*\right) = \sum_{i=1}^{\infty} \lambda_i \phi_i\left(\mathbf{z}\right) \phi_i\left(\mathbf{z}^*\right). \tag{2}$$

Note that this infinite series converges absolutely and uniformly on $\mathcal{D}' \times \mathcal{D}'$. Therefore, the Gaussian random field $X(\mathbf{z})$ defined on any $\mathcal{D} \subseteq \mathcal{D}'$ admits the following K-L expansion:

$$X\left(\mathbf{z}\right) = \overline{X}\left(\mathbf{z}\right) + \sum_{i=1}^{\infty} \sqrt{\lambda_i} \phi_i\left(\mathbf{z}\right) {}^1\theta_i, \tag{3}$$

where ${}^1\theta_i$ are independent standard normal random variables. This property, namely that the random field defined on $\mathcal{D} \subseteq \mathcal{D}'$ can be represented as the K-L expansion using $\{\lambda_i, \phi_i\}_{i=1}^{\infty}$ for the IEVP on $\mathcal{D}'$ (Eq.(1)), is called the domain independence property [4]. By truncating the K-L expansion, the Gaussian random field $X(\mathbf{z})$ can be approximated as

$$X\left(\mathbf{z}, {}^1\boldsymbol{\theta}\right) \approx \overline{X}\left(\mathbf{z}\right) + \sum_{i=1}^{M_1} \sqrt{\lambda_i} \phi_i\left(\mathbf{z}\right) {}^1\theta_i, \tag{4}$$

where ${}^1\boldsymbol{\theta} = \left[{}^1\theta_1, \ldots, {}^1\theta_{M_1}\right]^\top$. Note that while this approximation is optimal in the sense of minimizing the mean-square error in the general K-L expansion (i.e., $\mathcal{D} = \mathcal{D}'$) [6], such optimality does not hold for the K-L expansion using the domain independence property (i.e., $\mathcal{D} \subset \mathcal{D}'$). However, even without optimality, significant dimensionality reduction can be achieved [3, 7].

2.2 Parameterization

In the simultaneous estimation method, the spatial field and geometric features are parameterized by ${}^1\boldsymbol{\theta} \in \mathbb{R}^{M_1}$ and ${}^2\boldsymbol{\theta} \in \mathbb{R}^{M_2}$, respectively. The spatial field parameter ${}^1\boldsymbol{\theta}$, comprising random coefficients of the K-L expansion (Eq.(4)), follows a Gaussian prior $\mathcal{N}(\mathbf{0}, \mathbf{I}_{M_1})$. The geometry parameter

${}^2\boldsymbol{\theta}$ is defined according to the geometric feature of interest, which can include either direct definitions of simple shapes or more flexible parameterizations that control the degree of continuity, slope, and curvature of the boundary, such as B-splines. In this study, the prior of ${}^2\boldsymbol{\theta}$ is set as a Gaussian prior $p(\boldsymbol{\theta}) = \mathcal{N}(\boldsymbol{\mu}_2, \boldsymbol{\Sigma}_2)$ but must be truncated to ensure a physically sensible range. Finally, the prior of the complete set of parameters, $\boldsymbol{\theta} = [{}^1\boldsymbol{\theta}, {}^2\boldsymbol{\theta}]^\top$, can be represented as $\mathcal{N}(\boldsymbol{\mu}_{\boldsymbol{\theta}}, \boldsymbol{\Sigma}_{\boldsymbol{\theta}})$, where

$$\boldsymbol{\mu}_{\boldsymbol{\theta}} = \begin{bmatrix} \mathbf{0} \\ \boldsymbol{\mu}_2 \end{bmatrix}, \quad \boldsymbol{\Sigma}_{\boldsymbol{\theta}} = \begin{bmatrix} \mathbf{I}_{M_1} & \mathbf{0} \\ \mathbf{0} & \boldsymbol{\Sigma}_2 \end{bmatrix}. \tag{5}$$

In this study addressing the seepage flow problem, the K-L expansion (Eq.(4)) is applied not directly to the spatial field of hydraulic conductivity k, but to the logarithm of hydraulic conductivity u, represented as

$$u\left(\mathbf{z}, {}^1\boldsymbol{\theta}\right) = \log_{10}\left(k\left(\mathbf{z}, {}^1\boldsymbol{\theta}\right) - k_{\min}\right). \tag{6}$$

This formulation ensures that $k\left(\mathbf{z}, {}^1\boldsymbol{\theta}\right)$ remains greater than the lower bound $k_{\min} \geq 0$.

To estimate the geometric feature, note that the domain of the spatial field $\mathcal{D}$ depends on ${}^2\boldsymbol{\theta}$, i.e., $\mathcal{D}({}^2\boldsymbol{\theta})$. If the domain independence property is not applied, the IEVP in Eq.(1) must be solved repeatedly for each domain $\mathcal{D}({}^2\boldsymbol{\theta})$ to construct the K-L expansion. Additionally, gradient-based Bayesian inversion algorithms, such as Hamiltonian Monte Carlo (HMC), also require the expensive computation of a Moore-Penrose inverse to evaluate the gradient w.r.t the geometry parameters [2]. By utilizing the domain independence property, it is sufficient to solve the IEVP only once on a bounding domain $\mathcal{D}'$, which encompasses all possible realizations of $\mathcal{D}({}^2\boldsymbol{\theta})$, thereby significantly reducing the computational cost. In this study, the IEVP is numerically solved using the Nyström method. For details, see [1, 3].

2.3 Hyperparameters

The Hyperparameters for the spatial distribution are the covariance scale v, the correlation length l, and the mean $\overline{u}$ in the K-L expansion of u. In this study, the Gaussian autocovariance kernel is used:

$$C\left(\mathbf{z}, \mathbf{z}^*\right) = v \exp\left(\frac{-\left(\mathbf{z} - \mathbf{z}^*\right)^\top \left(\mathbf{z} - \mathbf{z}^*\right)}{2l^2}\right). \tag{7}$$

While a larger l allows for significant dimensionality reduction, it also smooths the spatial field [8] and does not capture abrupt changes. However, in the simultaneous estimation method, geometric features are modeled using ${}^2\boldsymbol{\theta}$. Thus, this approach can detect abrupt spatial changes while reducing dimensionality.

The hyperparameters for the geometric features are the mean $\boldsymbol{\mu}_2$ and the covariance matrix $\boldsymbol{\Sigma}_2$. These hyperparameters should be set so that the prior distribution is spread over a range that covers the true values. If the prior information is insufficient, the prior distribution should be non-informative. For example, set the mean $\boldsymbol{\mu}_2$ to the midpoint of the range of possible values for the parameter and set the variance $\boldsymbol{\Sigma}_2$ to be large.

3 BAYESIAN INFERENCE FOR INVERSION

3.1 Forward and observation models

Consider a soil domain $\mathcal{D}\left({}^2\boldsymbol{\theta}\right)$. Without sources, the steady seepage flow (ignoring transient effects) through $\mathcal{D}\left({}^2\boldsymbol{\theta}\right)$, governed by Darcy's law and the continuity equation, is represented as

$$\mathbf{v}\left(\mathbf{z}, {}^1\boldsymbol{\theta}\right) = -k\left(\mathbf{z}, {}^1\boldsymbol{\theta}\right) \nabla h\left(\mathbf{z}, {}^1\boldsymbol{\theta}\right), \tag{8}$$

$$\nabla \cdot \mathbf{v}\left(\mathbf{z}, {}^{1}\boldsymbol{\theta}\right) = 0, \tag{9}$$

where $\mathbf{z} \in \mathcal{D}\left({}^{2}\boldsymbol{\theta}\right)$, $h\left(\mathbf{z}, {}^{1}\boldsymbol{\theta}\right)$ is the total hydraulic head, $\mathbf{v}\left(\mathbf{z}, {}^{1}\boldsymbol{\theta}\right)$ is the seepage flow velocity, and $k\left(\mathbf{z}, {}^{1}\boldsymbol{\theta}\right)$ is the hydraulic conductivity. All boundaries are Dirichlet boundaries and are given as

$$h\left(\mathbf{z}\right) = h_0\left(\mathbf{z}\right), \tag{10}$$

where he term $h_0(\mathbf{z})$ is a known hydraulic head.

The forward problem is solved numerically using FEM during inversion. The nodes on $\mathcal{D}({}^{2}\boldsymbol{\theta})$ move following the update of $\mathcal{D}({}^{2}\boldsymbol{\theta})$, meaning that the nodal coordinate matrix can be represented as $\mathbf{Z}({}^{2}\boldsymbol{\theta})$. Consequently, the discretized form of Eq.(8) and Eq.(9) depends not only on ${}^{1}\boldsymbol{\theta}$ but also on ${}^{2}\boldsymbol{\theta}$, and is given as

$$\mathbf{K}(\boldsymbol{\theta})\mathbf{h}(\boldsymbol{\theta}) = \mathbf{q}(\boldsymbol{\theta}), \tag{11}$$

where $\mathbf{h}, \mathbf{q}$ are the global discretized hydraulic head and nodal flux vectors, and $\mathbf{K}$ is the global hydraulic conductivity matrix.

Observation data often contain noise, typically modeled as true values masked by Gaussian noise $\mathbf{r}_t \sim \mathcal{N}\left(\mathbf{0}, \mathbf{R}_t\right)$. Let $\mathbf{x}_t(\boldsymbol{\theta}) = \left[\mathbf{h}_t(\boldsymbol{\theta}), \mathbf{q}_t(\boldsymbol{\theta})\right]^{\top}$ be the state vector, and $\mathbf{H}$ be the measurement model matrix. Then, observations $\mathbf{y}_t$ are represented as

$$\mathbf{y}_t = \mathbf{H}\mathbf{x}_t(\boldsymbol{\theta}) + \mathbf{r}_t. \tag{12}$$

Here, the index $t \in \{1, \ldots, n\}$ refers to independent observation data collected under n different boundary conditions.

3.2 Bayesian parameter estimation

In Bayesian inference, the posterior distribution of $\boldsymbol{\theta}$ is to be computed by Bayes' theorem:

$$p\left(\boldsymbol{\theta}|\mathbf{y}\right) = \frac{p\left(\mathbf{y}|\boldsymbol{\theta}\right) p\left(\boldsymbol{\theta}\right)}{\int p\left(\mathbf{y}|\boldsymbol{\theta}\right) p\left(\boldsymbol{\theta}\right) \mathrm{d}\boldsymbol{\theta}}, \tag{13}$$

where $\mathbf{y}$ refers to $\{\mathbf{y}_1, \ldots, \mathbf{y}_n\}$, $p(\mathbf{y}|\boldsymbol{\theta})$ is the likelihood, and $p\left(\boldsymbol{\theta}\right)$ is the prior distribution. From Eq.(12), $p(\mathbf{y}|\boldsymbol{\theta})$ can be given as

$$p\left(\mathbf{y}|\boldsymbol{\theta}\right) = \prod_{t=1}^{n} p\left(\mathbf{y}_t|\boldsymbol{\theta}\right) = \prod_{t=1}^{n} \mathcal{N}\left(\mathbf{H}\mathbf{x}_t(\boldsymbol{\theta}), \mathbf{R}_t\right). \tag{14}$$

Substituting Eq.(14) and $p(\boldsymbol{\theta}) = \mathcal{N}(\boldsymbol{\mu}_{\boldsymbol{\theta}}, \boldsymbol{\Sigma}_{\boldsymbol{\theta}})$ into Eq.(13), $p\left(\boldsymbol{\theta}|\mathbf{y}\right)$ can be represented as

$$p\left(\boldsymbol{\theta}|\mathbf{y}\right) \propto \exp\left(-\varphi\left(\boldsymbol{\theta}\right)\right), \tag{15}$$

where $\varphi\left(\boldsymbol{\theta}\right)$ is the negative log density, defined as

$$\varphi\left(\boldsymbol{\theta}\right) \equiv \sum_{t=1}^{n} \frac{1}{2}\left(\mathbf{y}_t - \mathbf{H}\mathbf{x}_t\left(\boldsymbol{\theta}\right)\right)^{\top} \mathbf{R}_t^{-1}\left(\mathbf{y}_t - \mathbf{H}\mathbf{x}_t\left(\boldsymbol{\theta}\right)\right) + \frac{1}{2}\left(\boldsymbol{\theta} - \boldsymbol{\mu}_{\boldsymbol{\theta}}\right)^{\top} \boldsymbol{\Sigma}_{\boldsymbol{\theta}}^{-1}\left(\boldsymbol{\theta} - \boldsymbol{\mu}_{\boldsymbol{\theta}}\right). \tag{16}$$

In this study, $p\left(\boldsymbol{\theta}|\mathbf{y}\right)$ is obtained numerically using HMC, which uses the gradient of the negative log density $\frac{\partial \varphi}{\partial \boldsymbol{\theta}}$ to enhance sampling efficiency. The roots of this gradient are $\frac{\partial u}{\partial {}^1\boldsymbol{\theta}}$ and $\frac{\partial \mathbf{Z}}{\partial {}^2\boldsymbol{\theta}}$, which propagate as follows to obtain $\frac{\partial \varphi}{\partial {}^1\boldsymbol{\theta}}$ and $\frac{\partial \varphi}{\partial {}^2\boldsymbol{\theta}}$, respectively:

$$\frac{\partial \varphi(\boldsymbol{\theta})}{\partial \boldsymbol{\theta}} \leftarrow \frac{\partial \mathbf{x}_t(\boldsymbol{\theta})}{\partial \boldsymbol{\theta}} \leftarrow \frac{\partial \mathbf{K}(\boldsymbol{\theta})}{\partial \boldsymbol{\theta}} \leftarrow \frac{\partial k(\mathbf{z}({}^2\boldsymbol{\theta})), {}^1\boldsymbol{\theta})}{\partial \boldsymbol{\theta}} \leftarrow \frac{\partial u(\mathbf{z}, {}^1\boldsymbol{\theta})}{\partial {}^1\boldsymbol{\theta}}$$
$$\nwarrow \frac{\partial u(\mathbf{z}({}^2\boldsymbol{\theta}), {}^1\boldsymbol{\theta})}{\partial {}^2\boldsymbol{\theta}} \leftarrow \frac{\partial \mathbf{Z}({}^2\boldsymbol{\theta})}{\partial {}^2\boldsymbol{\theta}}.$$

For details of the HMC flow and each gradient computation, see [3].

4 NUMERICAL STUDY

This study considers a 1D steady vertical seepage flow in the soil domain $\mathcal{D}'$ as shown in Fig. 1(A). The target soil domain $\mathcal{D}'$ consists of two domains: sandy layers $\mathcal{D}_1 = \{z : 0 \leq z < 4.1\} \cup \{z : 5.8 < z \leq 10\}$ and a clay seam $\mathcal{D}_2 = \{z : 4.1 \leq z \leq 5.8\}$. The spatial field of hydraulic conductivity is shown in Fig. 1(B), and let $k_i(z)$ and $u_i(z)$ be the hydraulic conductivity and logarithmic hydraulic conductivity in $\mathcal{D}_i$ $(i = 1, 2)$, respectively. Dirichlet boundary conditions (BCs) are implemented such that the hydraulic head at the ground surface varies as $h(z = 0, t) = 0.1 + 0.01(t - 1)$ for $t \in \{1, ..., 21\}$, while $h(z = 10, t) = 0$ is kept fixed. Observation data consist of the hydraulic head measured at 6 points ($z = 0.25, 0.75, 4.75, 5.25, 9.25, 9.75$ represented by red cross marks in Fig. 1(A)) and the water inflow rate measured at the top for 21 sets of BCs. These observations were obtained by masking Gaussian noise with true values. The true values are obtained numerically by solving the forward problem for the true condition on a mesh with 200 equally spaced finite elements in $\{z : 0 \leq z \leq 10\}$.

The targets of inversion are k_i and interfaces of two domains ${}^2\boldsymbol{\theta} = [{}^2\theta_1, {}^2\theta_2]^\top = [z_{\text{upper}}, z_{\text{lower}}]^\top$. The spatial fields of hydraulic conductivity $k_i(z)$ are represented via the K-L expansion of $u_i(z)$ and are parameterized by ${}^1\boldsymbol{\theta}_i$. Thus, ${}^1\boldsymbol{\theta} = [{}^1\boldsymbol{\theta}_1, {}^1\boldsymbol{\theta}_2]^\top$. Two domains $\mathcal{D}_i$ depend on ${}^2\boldsymbol{\theta}$, represented as follows:

$$\mathcal{D}_1({}^2\boldsymbol{\theta}) = \left\{z : 0 \leq z < {}^2\theta_1\right\} \cup \left\{z : {}^2\theta_2 < z \leq 10\right\},\ \mathcal{D}_2({}^2\boldsymbol{\theta}) = \left\{z : {}^2\theta_1 \leq z \leq {}^2\theta_2\right\}. \tag{17}$$

To avoid realizations of a non-physical domain, constraints $1.05 < {}^2\theta_1 < 4.7$ and $5.3 < {}^2\theta_2 < 8.95$ are imposed on ${}^2\boldsymbol{\theta}$. The discretized soil domain consists of 41 nodes (Fig. 1(C)), with the position of each given as follows:

$$z_i({}^2\boldsymbol{\theta}) = \begin{cases} 0.25(i-1) & (1 \leq i \leq 5, 20 \leq i \leq 22, 37 \leq i \leq 41) \\ 1 + \frac{{}^2\theta_1 - 1}{8}(i-5) & (6 \leq i \leq 12) \\ {}^2\theta_1 & (i = 13) \\ {}^2\theta_1 + \frac{4.75 - {}^2\theta_1}{7}(i-13) & (14 \leq i \leq 19) \\ 5.25 + \frac{{}^2\theta_2 - 5.25}{7}(i-22) & (23 \leq i \leq 28) \\ {}^2\theta_2 & (i = 29) \\ {}^2\theta_2 + \frac{9 - {}^2\theta_2}{8}(i-29) & (30 \leq i \leq 36). \end{cases} \tag{18}$$

This mapping always generates a mesh that satisfies $z_i < z_{i+1}$, ensuring a physically valid mesh configuration.

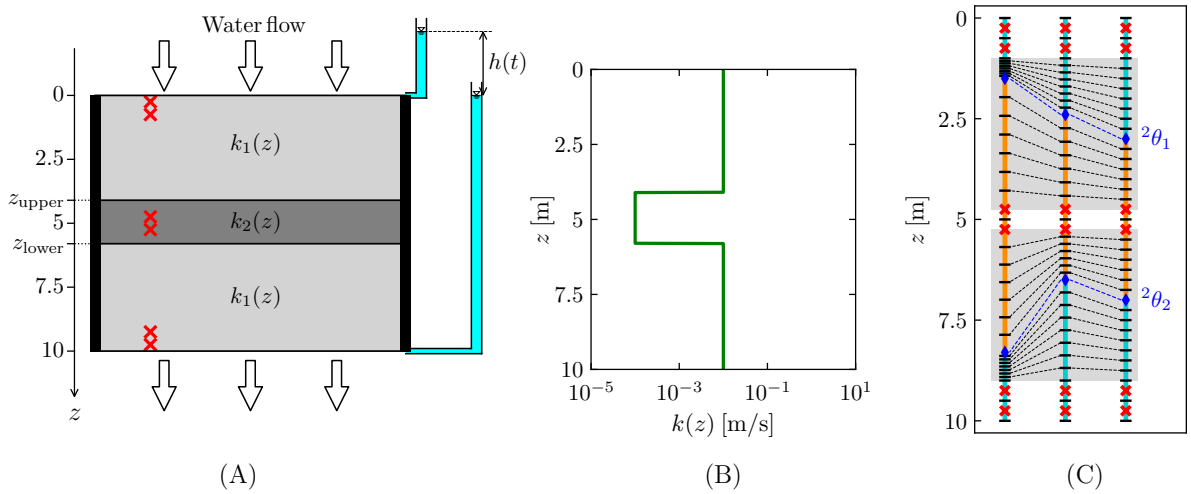

Figure 1: (A) Target domain with a thin clay layer $\mathcal{D}_2$ sandwiched in between two sandy layers $\mathcal{D}_1$. (B) True hydraulic conductivity field. (C) Definition of how nodes move: Only nodes in the gray area move, while observation points (red cross marks) remain fixed. The cyan and orange lines correspond to $\mathcal{D}_1$ and $\mathcal{D}_2$, respectively.

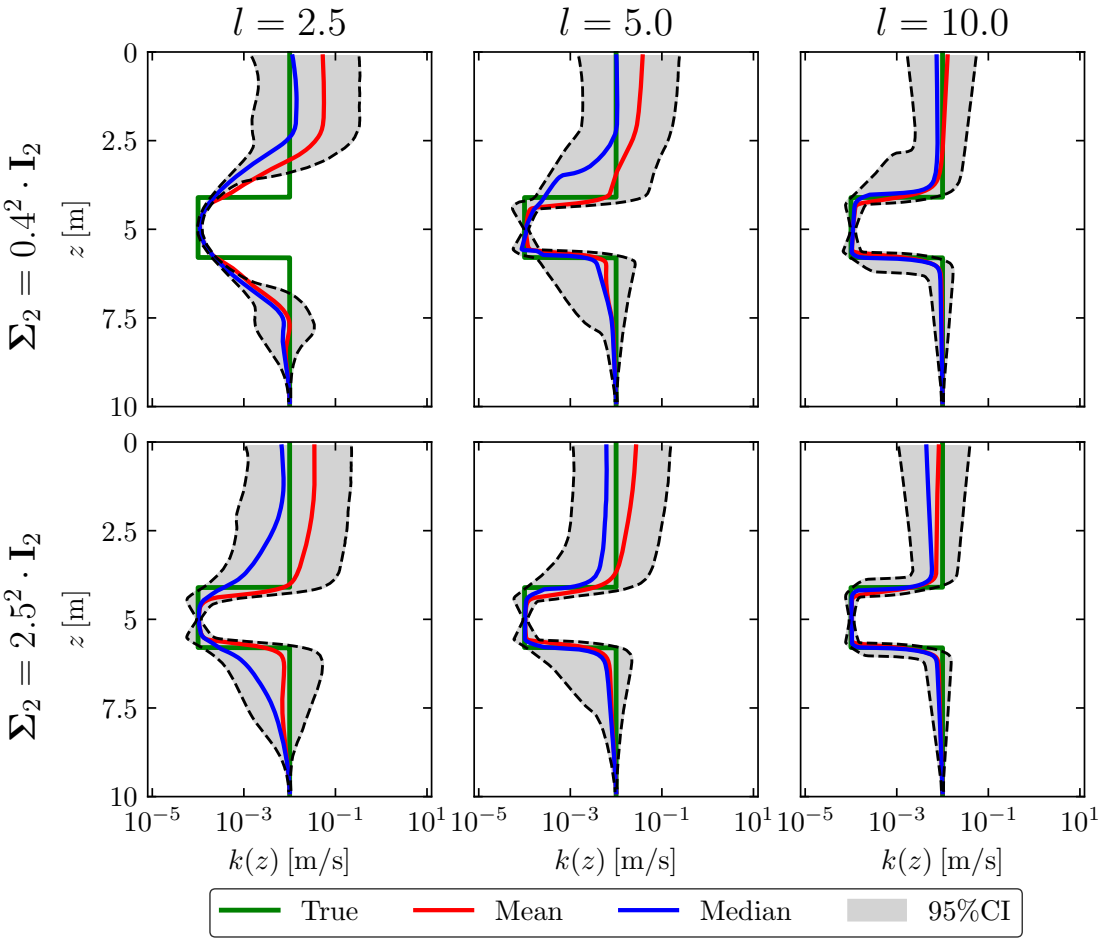

Figure 2: Estimated hydraulic conductivity fields for 6 different hyperparameter sets

Hyperparameters for u_1 and u_2 are chosen to be the same value: the mean $u = -3$, scale $v = 1$, and correlation length $l \in \{2.5, 5.0, 10.0\}$. For hyperparameters of $\boldsymbol{\mu}_2$, set the mean to $\boldsymbol{\mu}_2 = [2.5, 7.5]^\top$ and choose covariance matrix $\boldsymbol{\Sigma}_2 \in \{0.4^2 \cdot \mathbf{I}_2,\ 2.5^2 \cdot \mathbf{I}_2\}$. Thus, there are 6 hyperparameter sets based on the different choices of $(l, \boldsymbol{\Sigma}_2)$.

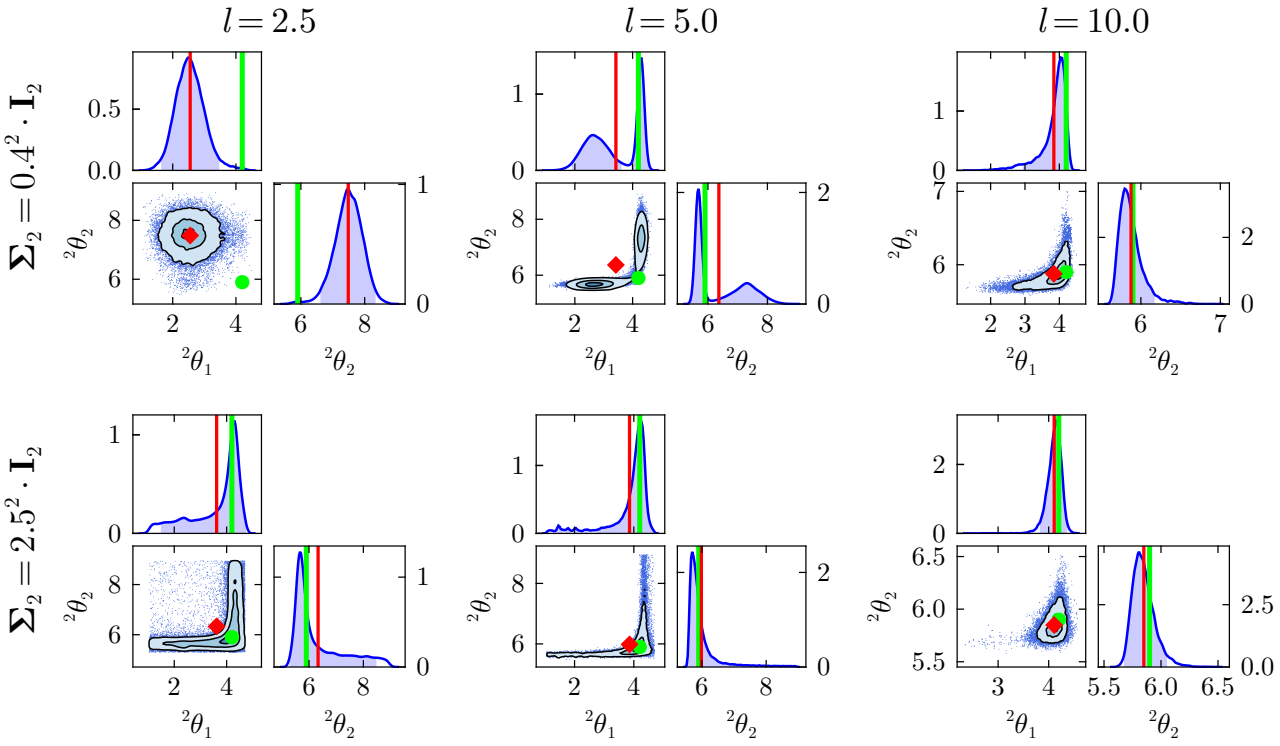

Figure 3: Marginal distributions of $p\left({}^2\boldsymbol{\theta}|\mathbf{y}\right)$. The red diamond and red line represent the mean value of the posterior distribution. The green circle and green line represent the true value of ${}^2\boldsymbol{\theta} = [4.1, 5.8]^\top$. In 1D distribution plots, the blue color area represents the 95% High Probability Density (HPD) regions, and in 2D distribution plots, the three contours indicate the 5%, 50%, and 95% HPD regions.

A total of 40000 posterior samples were generated using HMC, and results of the spatial field of hydraulic conductivity are shown in Fig. 2. The bottom row of Fig. 2 corresponds to the case for $\boldsymbol{\Sigma}_2 = 2.5^2 \cdot \mathbf{I}_2$. In this setting, the prior $\mathcal{N}(\boldsymbol{\mu}_2, \boldsymbol{\Sigma}_2)$ can be regarded as unbiased and covers the possible value range of ${}^2\boldsymbol{\theta}$. For all choices of l, the 95% credible intervals (CIs) capture the true field. In particular, for $l = 5.0$ and $l = 10.0$, both the posterior mean and the median closely align with the true distribution. The width of the 95% CI increases as l decreases. This is because higher-frequency spatial fields, which have greater expressiveness, can produce forward responses that match observations while differing from the true field. In contrast, the top row of Fig. 2 shows the results for $\boldsymbol{\Sigma}_2 = 0.4^2 \cdot \mathbf{I}_2$, where the prior $\mathcal{N}(\boldsymbol{\mu}_2, \boldsymbol{\Sigma}_2)$ is biased near ${}^2\boldsymbol{\theta} = [2.5, 7.5]^\top$ and is thus misaligned with the true interface locations. In the case of $l = 2.5$, the 95% CI fails to fully encompass the true field. For $l = 5.0$, the 95% CI is slightly wider in the upper half of the region, and the jump in the median field shifts upward compared to the case of $\boldsymbol{\Sigma}_2 = 2.5^2 \cdot \mathbf{I}_2$. However, for $l = 10.0$, the 95% CI remains sufficiently narrow, and the mean and median fields coincide with the true field. This indicates that even if the priors of the geometry parameter have biases, it is possible to obtain accurate results by choosing an appropriate correlation length.

The influence of the prior distribution is also shown in the posterior distribution of the geometry parameters (Fig. 3). In the case of $\mathbf{\Sigma}_2 = 2.5^2 \cdot \mathbf{I}_2$, the high-density region of the posterior is located around the true values. In contrast, for $\mathbf{\Sigma}_2 = 0.4^2 \cdot \mathbf{I}_2$, the influence of the prior tends to be larger. For $l = 2.5$, the marginal distribution has a high-density region near the prior mean $\boldsymbol{\mu}_2 = [2.5, 7.5]^\top$. For $l = 5.0$, the posteriors become bimodal distributions due to the competing influences of both the prior and the likelihood. This is because spatial fields with a smaller correlation length are so expressive that they can achieve high likelihood without shifting the inaccurate and strongly biased geometry parameters to their true values, thereby rendering the geometry parameters meaningless. In contrast, for $l = 10.0$, the high-density region closely aligns with the true value, since spatial fields with a longer correlation length are less expressive, making it impossible to increase the likelihood without shifting the geometry parameters toward their true values.

These results emphasize the importance of selecting an appropriate l, which directly affects the dimensionality of the estimated parameter. By selecting the largest possible l that can represent the target field, the dimensionality of the parameters can be reduced. This means that by simplifying the inversion model and avoiding excessive expressiveness, both the K-L expansion and the geometry parameters can perform effectively, allowing for more accurate estimation.

5 CONCLUSION

This study investigates the influence of prior on estimation results in simultaneous geometry and spatial field estimation. This simultaneous estimation approach enables flexible modeling by overcoming the drawback of spatial field smoothing, which occurs as a side effect of dimensionality reduction through the Karhunen-Loève (K-L) expansion, through the introduction of geometry parameters. This study shows that the inverse analysis for 1D seepage flow problem demonstrated that selecting appropriate hyperparameters, especially correlation length, is crucial for accurate estimation. A small correlation length increases the expressiveness of the spatial field, allowing multiple plausible solutions consistent with observations, but resulting in the larger variance of estimated parameters. Furthermore, the increased expressiveness of the spatial field can render the geometry parameters meaningless, preventing the accurate detection of abrupt spatial changes. For both K-L expansion and geometry parameters to perform effectively, it is necessary to avoid excessive representation of the spatial field. Therefore, selecting the largest feasible correlation length that still captures essential spatial features is quite important for balancing dimensionality reduction and estimation accuracy. Additionally, it has been revealed that if an appropriate correlation length is selected, the prior distribution of geometric parameters can still be estimated with high accuracy, even if the prior distribution of geometric parameters is inaccurate and strongly biased.

REFERENCES

[1] W. Betz, I. Papaioannou, D. Straub, Numerical methods for the discretization of random fields by means of the Karhunen–Loève expansion, Computer Methods in Applied Mechanics and Engineering 271 (2014) 109–129. doi:10.1016/j.cma.2013.12.010.

[2] M. C. Koch, M. Osugi, K. Fujisawa, A. Murakami, Hamiltonian Monte Carlo for Simultaneous Interface and Spatial Field Detection (HMCSISFD) and its application to a piping zone interface detection problem, International Journal for Numerical and Analytical Methods in Geomechanics 45 (17) (2021) 2602–2626. doi:10.1002/nag.3279.

[3] T. Shibata, M. C. Koch, I. Papaioannou, K. Fujisawa, Efficient bayesian inversion for simultaneous estimation of geometry and spatial field using the karhunen-loève expansion, Computer Methods in Applied Mechanics and Engineering 441 (2025) 117960. doi:https://doi.org/10.1016/j.cma.2025.117960.

[4] S. Pranesh, D. Ghosh, Faster computation of the Karhunen–Loève expansion using its domain independence property, Computer Methods in Applied Mechanics and Engineering 285 (2015) 125–145. doi:10.1016/j.cma.2014.10.053.

[5] R. M. Neal, MCMC Using Hamiltonian Dynamics, in: Handbook of Markov Chain Monte Carlo, Chapman and Hall/CRC, 2011, pp. 113–162.

[6] R. G. Ghanem, P. D. Spanos, Stochastic Finite Elements: A Spectral Approach, revised edition Edition, Dover Publications, Minneola, N.Y, 2012.

[7] I. Papaioannou, Non-intrusive finite element reliability analysis methods, Ph.D. thesis, Technische Universität München (2012).

[8] C. K. Williams, C. E. Rasmussen, Gaussian Processes for Machine Learning, Vol. 2, MIT press Cambridge, MA, 2006.